Trinity College
Trinity College Digital Repository

Faculty Scholarship

9-2013

Design and implementation of a fs-resolved transmission electron microscope based on thermionic gun technology [post-print]

L. Piazza

D. J. Masiel

T. LaGrange

B. W. Reed

Brett Barwick
Trinity College, brett.barwick@trincoll.edu

Follow this and additional works at: http://digitalrepository.trincoll.edu/facpub

Part of the Physics Commons

Design and implementation of a fs-resolved transmission electron microscope based on thermionic gun technology

L. Piazza*[1], D. J. Masiel[2], T. LaGrange[3], B. W. Reed[3], B. Barwick[4], Fabrizio Carbone[1]

[1]*Laboratory for Ultrafast Microscopy and Electron Scattering (LUMES), ICMP,*

Ecole polytechnique fédérale de Lausanne, CH-1015 Lausanne, Switzerland.

[2]*Integrated Dynamic Electron Solutions, Inc.,*

455 Bolero Drive, Danville, Califonia 94526 USA

[3] *Condensed Matter and Materials Division Physical and Life Sciences Directorate,*

Lawrence Livermore National Laboratory,

P.O. Box 808; L-356, Livermore, CA 94550, USA and

[4]*Department of Physics, Trinity College,*

300 Summit St., Hartford, Connecticut 06106 USA

Abstract

In this letter, the design and implementation of a femtosecond-resolved ultrafast transmission electron microscope is presented, based on a thermionic gun geometry. Utilizing an additional magnetic lens between the electron acceleration and the nominal condenser lens system, a larger percentage of the electrons created at the cathode are delivered to the specimen without degrading temporal, spatial and energy resolution significantly, while at the same time maintaining the femtosecond temporal resolution. Using the photon-induced near field electron microscopy effect (PINEM) on silver nanowires the cross-correlation between the light and electron pulses was measured, showing the impact of the gun settings and initiating laser pulse duration on the electron bunch properties. Tuneable electron pulses between 300 fs and several ps can be obtained, and an overall energy resolution around 1 eV was achieved.

* Corresponding author

The extension of transmission electron microscopy to the fourth dimension, time, has taken several steps to reach the ns to fs resolution domain [1–5], proving to be dramatically effective in the investigation of light induced phenomena in a variety of systems [6–11] and spanning areas of research like physical chemistry [12, 13], biophysics [14], nanophotonics [15], condensed matter physics [16] and materials science [17, 18]. Unlike a conventional TEM, high time resolution electron microscopes take advantage of laser generated ultrashort pulses of electrons to probe the specimen. To achieve femtosecond time resolution with the low energy spread desired for real-space imaging, the simplest technique is to allow each electron pulse to contain at most one electron [19]. This requirement imposes the use of a very low average current in the TEM, thus sacrificing signal in order to obtain the best possible spatial and temporal coherence.

Currently, there are two main approaches to time resolved electron microscopy: femtosecond ultrafast electron microscopy (UEM) which uses stroboscopic "single" electron pulses to study ultrafast dynamics [19, 20] and the dynamic transmission electron microscope (DTEM) which uses electron pulses containing more than 10^8 electrons to acquire "single-shot" images with nanosecond exposure times [17, 21, 22]. This letter focuses on a new microscope that is optimized for operation in the femtosecond mode, or UEM, that utilizes a combination of a thermionic source with a Wehnelt and an extra condenser lens. In fs-resolved machines, it is important to keep the current density very low to avoid the temporal broadening of the electron pulses during propagation due to space charge. In this low current or "single" electron regime, the average beam current is a few orders of magnitude lower when compared to the conventional continuous wave (CW) electron beam in thermionic mode. For example, when operating at 1 MHz with 1 ps electron pulses, a current is present in the microscope only for 1 μs out of every second. This greatly decreases the signal that is available for imaging, diffraction or spectroscopy. Unfortunately, the increase in the electron energy spread and pulse duration, caused by space charge and Boersch effects, happens at the source and in the accelerator section, where the electrons are moving relatively slowly. In a standard TEM design, the current throughput between the gun and the sample is typically only a few percent at most (and often much less). Thus if an average pulse has a single electron when it reaches the sample, very likely it had tens or even hundreds to thousands of electrons when it was emitted, and the presence of these unused electrons may substantially worsen the time and energy resolution. To optimize the perfor-

mance in fs mode, two things must be done: (1) adjust the conditions at the electron gun so that it only emits a small excess of electrons beyond those that are used to form an image or spectrum and (2) modify the condenser lens system to capture a very large fraction of the emitted electrons. To satisfy the first task, we systematically vary the laser pulse energy, laser pulse duration and the bias voltage on the Wehnelt electrode (which, for a thermionic source, acts as a feedback-stabilized electron focusing and suppression optical element). As we vary these parameters, we measure the signal level, pulse duration, and energy spread in order to understand how to optimize performance for any given experiment. To do the second, we add a large, weakly focusing condenser lens, called the C0 lens since it precedes the standard C1 condenser lens, similarly to the design described in [23]. The Wehnelt is an electrostatic lens which works by decelerating, then reaccelerating the electron beam while it is still at a very low energy, greatly increasing dispersion. Any electrostatic lens in the upper regions of the accelerator would similarly tend to degrade the pulse duration. Whereas the C0 lens is a magnetic lens operating on the fully accelerated beam and thereby has much less detrimental effects on the pulse duration. The C0 lens is crucial for the operation of the Wehnelt based UEM, because, as we show below, the shortest duration electron pulses are obtained with zero or low Wehnelt bias; this in turn does not efficiently couple the electrons down the column, which dramatically reduces the electron counts. The C0 lens is used to get a majority of the electrons that exit the accelerator to reach the sample, thus recovering the signal lost because of the Wehnelt settings. Moreover, ad hoc combinations of electron-pulse duration and coherence can be achieved by independently controlling the Wehnelt and C0 voltages. In fact, since brightness is conserved, signal increases at the expense of spatial coherence and hence can reduce spatial resolution. It should be mentioned as well that in previous reports describing the C0 lens operation with nanosecond electron pulses the primary advantage was its ability to increase current for single shot imaging; in the application reported here, this lens's primary use is to prevent space-charge effects in the gun region by providing a combination of electron-collection and acceleration that optimizes the duration and energy spread of fs-electron bunches. As we shall show below, the impact of such a modification on the performance in static imaging mode is minimal. With this modified system, we show that few-hundred-fs time resolution can be achieved with sufficient electron counts for imaging, diffraction, and EELS. This approach delivers similar results to a UEM with a modified FEG module which uses the extractor and suppressor lens system to control the

emission properties of the photo-current; here, we show that in our microscope the simpler combination of the Wehnelt and C0 allows the direct control of electron pulse duration and beam current. This ability allows the microscope to be optimized for the demands of each experiment. It has to be noted that conventional field-emission guns come with voltage controllers that often forbid independent tuning of the extractor/suppressor lenses, resulting in a somewhat limited tuneability of the instrument [20].

The femtosecond laser used in the setup is a "KMLabs Wyvern X" Ti:Sapph amplified laser pumped by three Finesse CW green pump lasers for a total maximum pump power of about 40 W. It delivers 5 W of average power at 800 nm wavelength, 80 fs pulse duration, and repetition rates between 200 kHz and 2 MHz. The beam is split into two paths: one is frequency tripled to generate the UV probe beam, while the other is used to pump the specimen. The laser pulses are sent to the microscope to allow fs time-resolved electron microscopy (dynamical) operation. The microscope is a modified JEOL 2100 TEM with a Gatan Quantum GIF electron energy loss spectrometer (EELS). Two optical ports have been added to the microscope, two mirrors have been placed inside the column and an additional magnetic lens has been placed between the acceleration region and the C1 lens. The upper optical window located in an additional column section allows the UV (266 nm) laser pulses to enter the microscope, where it is reflected on a movable holed aluminum mirror. After the UV is reflected up the column it hits a 30 μm flat LaB$_6$ tip, creating electron pulses through the photoelectric effect. A second optical window located near the specimen allows an additional laser beam to enter the column, where it hits a mirror that is placed on the top of the objective lens pole-piece. This second laser beam after reflection on the mirror is focused onto the specimen. The additional C0 magnetic lens allows the electrons to be more efficiently coupled down the column. A schematic of the modification is presented in Fig. 1. In the right panel of Fig. 1 two high-resolution images taken in thermionic emission mode before (top) and after (bottom) the modification are shown. After the modification, a slight blurring is visible towards the edges of the image, resulting in a slightly lower spatial resolution. However, lattice fringes are visible in both images proving that the modification itself only has a minor impact on the conventional performance of the TEM. When the C0 lens voltage is increased, an increased electron intensity is achieved at the expense of the spatial resolution. Also, for dynamical operation a 30 μm flat LaB$_6$ tip is used instead of the standard conic one, also resulting in a somewhat reduced spatial resolution. For these

reasons, in a realistic time-resolved experiment, a spatial resolution around 1 nm is to be expected. It is important to stress at this point that in time-resolved experiments the overall final spatial resolution does not depend solely on the imaging capability of the microscope but also on the mechanical response of the sample to the exciting pulses and the possible photoemitted charge present on its surface [24, 25].

While the microscope can be operated in thermionic mode, where it gives performances similar to a standard machine, we will focus here on its operation in femtosecond pulsed mode operation. The two parameters that require optimization while in femtosecond pulsed mode are total current and the energy resolution (width of the zero loss peak (ZLP)). One important characteristic of the JEOL 2100 TEM is that the voltage on the Wehnelt can be adjusted directly and does not rely on the feedback current provided by the electron beam. That is, there is a static bias voltage continuously applied to the Wehnelt that can be independently varied, which is crucial for optimizing pulsed electron parameters. This voltage can be adjusted from around 0 V to roughly 1000 V, even with the emission current equal to zero, and the change in this voltage when the filament emits in thermionic mode is relatively small. The characteristic response time of the resistive feedback is much longer than the photoemitted pulse duration. When a high bias voltage is used on the Wehnelt, electrons emitted from the center of the tip are selected and coupled down the column. This typically results in better beam coherence and lower energy spread in the ZLP, but because the Wehnelt voltage tends to decelerate the electrons at the cathode, the pulse suffers from space-charge effects, resulting in longer pulses. On the contrary, if very low or no bias voltage is applied to the Wehnelt, electrons from a larger region of the cathode are accepted, the energy spread of the ZLP is larger and the coherence of the beam is lower, but electron pulses with durations of a few hundred fs can be obtained (as will be shown in Fig. 4). In Fig. 2, the effect of the bias voltage on the beam properties is visible. In all the experiments the strength of the C0 lens is kept at its optimal value to maximize counts. The UV beam from the laser is directed to the cathode via a 1 m focal length optical lens. The spot-size at the LaB_6 tip is estimated to be between 100 and 150 μm in diameter. The repetition-rate of these experiments was 1 MHz. In Fig. 2 A, the electron counts as a function of the UV power used to photoemit electrons from the cathode are shown; a 0 V bias on the Wehnelt lens was set. An image of the tip is taken for different UV power values, top panels of Fig. 2. The electron counts are estimated on the detector

by integrating the intensity of all the pixels in the images and then converting pixel counts to electron counts. At low UV power, the electron counts are found to increase linearly with the laser power as expected for the photoelectric effect. However, a saturation in the counts is observed beyond 150 electrons/pulse on the detector. It is interesting to notice that above 1 mW of illuminating UV power, corresponding to approximately 30 electrons per pulse, the image of the tip becomes blurred (Fig. 2 A and central top panel), and the energy width of the ZL peak begins to significantly broaden, Fig. 2 B. The width in energy of the ZL peak displayed as a function of the UV power for two different Wehnelt bias voltages also shows a divergence beyond 1 mW of UV power for the 0 V bias setting. At higher UV power, the width of the ZL becomes several eV, and the image of the tip becomes a cloud of charge with no details distinguishable (Fig 2, top right panel), testifying to the abrupt onset of space-charge effects already at very low currents.

It is interesting to notice that for a high voltage on the Wehnelt (350 V, Fig. 2 B), a higher number of electrons in the pulses does not result in a broader energy distribution. This suggests, and will be verified below, that the electron pulses have fairly long durations, so that the space-charge effects are less severe due to a low instantaneous electron density. This is consistent with the fact that a higher bias voltage reduces the acceleration of the electrons at the cathode, as discussed above. Instead, at low bias voltages, the energy spread of the beam drastically increases with electron density, suggesting that in realistic time-resolved operation a very low current has to be maintained to keep both a short pulse duration and a narrow energy distribution. The so-called "single electron regime" is attained by lowering the UV power on the cathode until the ZLP reaches its minimum width, 1 eV (corresponding to an UV illumination of less then 1 mW at 1 MHz repetition rate in Fig. 2 B).

The duration of the electron pulses is characterized via photon-induced near field electron microscopy (PINEM) [15, 26–32]. When electrons and photons are overlapped spatially and temporally on a nanostructure, the evanescent field photoinduced at the edges of the latter interacts with the electrons allowing them to absorb and emit photons from the pump laser beam [15]. This results in sideband peaks spaced by an energy corresponding to the pump photon energy on both the energy gain and loss sides of the ZLP [15]. Because the surface charge density waves that mediate this interaction typically have very short lifetimes relative to the excitation pulse durations, the temporal duration of the PINEM effect is a

cross-correlation between the laser pulse and the electron pulse, while they are both in the vicinity of the nanostructure. To measure the pulse duration using the PINEM effect a specimen of silver nanowires, whose average diameter was around 100 nm with average lengths of a few μm was used (see Fig. 3 D). The laser pulse duration was varied from 100 fs to 2 ps, at a wavelength of 800 nm (1.55 eV photons), with a repetition rate of 1 MHz and a fluence as high as 10 mJ/cm^2. The delay between the IR pump pulses and the photoemitting UV pulses is changed via a computer-controlled optical delay-line. In Fig. 3 A the time-energy dependence of the EEL spectrum through the silver nanowire sample is displayed. The bias voltage in the Wehnelt lens was set to 300 V. In Fig. 3 B the energy spectrum before the arrival of the laser pulses (red line) and at the time of coincidence between electrons and photons (blue line) is shown. The sideband peaks of the PINEM effect are clearly distinguishable and are separated by 1.55 eV as expected. We can count up to 18 peaks on each side of the zero-loss peak, corresponding to a gain or a loss in the kinetic energy of the electrons by as much as 27.9 eV. In Fig. 3 C, the temporal evolution of one of the satellite peaks is displayed. The FWHM of the whole cross-correlation is around 1.5 ps, similar to what was reported in [15]. In Fig. 3 D, an image of the silver nanowires taken integrating for 2 seconds the photoelectron beam is shown. These spectra show that our instrument has around 1 eV energy-resolution in pulsed operation, similar to the resolution of the conventional CW TEM and sufficient to look at both low-energy loss plasmons [13] and multiplets effects in core levels [33].

The electron pulse duration can be varied by changing either the initial laser pulse duration or bias voltage on the Wehnelt. In particular, the electron pulse duration is very sensitive to the bias voltage, for the reasons discussed above. In Fig. 4, the evolution of the PINEM cross-correlation is shown as a function of the laser pulse duration and the bias voltage. In Fig. 4 A, the temporal evolution of the ZLP of the PINEM spectrum for a bias voltage of 300 V is shown at different values of the laser pulse duration. Clearly, when the laser pulses are longer than the electron pulses, a longer cross-correlation is observed (magenta trace, 2.5 ps). Instead, a sharper effect is observed when the laser and electron pulses durations are equally matched. This happens at a value around 750 fs, delivering a good estimate of the electron bunch duration. In Fig. 4 B, the temporal evolution of the PINEM signal for a bias voltage of 0 V at different durations of the laser pulses is displayed. In this case, an electron/light cross-correlation as short as 480 fs is observed, confirming the

idea that the best time-resolution, i.e. shorter electron pulses, is obtained for the maximum acceleration from the cathode (no bias voltage on the Wehnelt lens). The dependence of the cross correlation FWHM on the laser pulses width is shown in Fig. 4 C for the two bias voltages used, and in Fig. 4 D the duration of the electron pulses is plotted against the bias voltage. An extra experiment was performed at a high bias (600 V), delivering pulses as long as 5 ps. To the best of our knowledge, the dependence of the PINEM effect on the initiating laser duration has never been reported, and it also provides an interesting insight in the relation between the photoinduced field duration and its interaction with the electrons. It is not immediately obvious for instance why a longer laser pulse produces a shorter cross-correlation. One possible explanation may be that the PINEM effect is higly nonlinear, and is enhanced when a strong electric field is present during the whole duration of the electron pulse, i.e. giving the sharpest effect when light and electron pulses durations coincide.

The overall duration of the PINEM effect strongly depends on the voltage placed on the Wehnelt. Moreover, when changing the Wehnelt voltage, a shift of the temporal coincidence between electrons and photons is also observed, as a consequence of the different acceleration times for the photoemitted electrons. The temporal broadening is overcome by reducing the Wehnelt bias voltage to zero, which results in greatly reduced signal. However, this signal can be recovered by using the C0 lens to better couple the electrons down the column.

In conclusion, we demonstrate the ability to modify a commercial Wehnelt-based JEOL 2100 TEM for fs-pulsed operation. Having flexible control of the Wehnelt lens bias voltage and the addition of an electromagnetic lens right after the acceleration stage, we demonstrate the ability to obtain fs time-resolution, 1 eV energy resolution while maintaining a good overall brightness of the instrument. Also, the electron pulses properties in terms of duration and energy spread can be independently controlled via the bias voltage and the control of the photoemission yield, making this tool highly versatile.

[1] G.V. Spivak, O.P. Pavlyuchenko, V.I. Petrov. Electron microscopic observation of alterations of the domain structure of magnetic films. Bulletin of the Academy of Sciences of the USSR Physical Series **30**, 822 (1966).

[2] O. Bostanjoglo, T. Rosin. Stroboscopic study on ultrasonic activity in electron- microscope. Mikroskopie **32**, 190 (1976).

[3] B.J. Siwick, J.R. Dwyer, R.E. Jordan, R.J.D. Miller. Ultrafast electron optics: Propagation dynamics of femtosecond electron packets. Journal of Applied Physics, **92** (2002).

[4] M. Aidelsburger, F. O. Kirchner, F. Krausz, P. Baum. Single-electron pulses for ultrafast diffraction. Proc. Natl. Acad. Sci. **107** (2010).

[5] Y. Wang; N. Gedik. Electron Pulse Compression With a Practical Reflectron Design for Ultrafast Electron Diffraction. IEEE Journal of Selected Topics in Quantum Electronics **18** (2012).

[6] Four-Dimensional Electron Microscopy. A.H. Zewail, Science **328** 187 (2010)

[7] A perspective on novel sources of ultrashort electron and X-ray pulses. F. Carbone, P. Musumeci, O.J. Luiten, C. Hebert, Chemical Physics, **392**, 1 (2012)

[8] Modern electron microscopy resolved in space, energy and time. F. Carbone, E. Phys. J.-Appl. Phys.**54**, 33503 (2011)

[9] Design and implementation of a flexible beamline for fs electron diffraction experiments. G.F. Mancini, B. Mansart, S.Pagano, B. van der Geer, M. de Loos, F. Carbone, Nucl. Instr. and Meth. in Phys. Res. A, **691**, 113 (2012).

[10] J. B. Hastings, F. M. Rudakov, D. H. Dowell, J. F. Schmerge, J. D. Cardoza, J. M. Castro, S. M. Gierman, H. Loos, P. M. Weber. Ultrafast time-resolved electron diffraction with megavolt electron beams. APL **89** (2006).

[11] S. Tokita, S. Inoue, S. Masuno, M. Hashida, S. Sakabe. Single-shot ultrafast electron diffraction with a laser-accelerated sub-MeV electron pulse. APL **95** (2009).

[12] Dynamics of Chemical Bonding Mapped by Energy-Resolved 4D Electron Microscopy. F. Carbone, O.-H. Kwon, and A. H. Zewail Science **325**, 181 (2009).

[13] EELS femtosecond resolved in 4D ultrafast electron microscopy F. Carbone, et al. Chem. Phys. Lett. **468** 107 (2009).

[14] Biological Imaging with 4D Ultrafast Electron Microscopy. J. Flannigan, B. Barwick, and A. H. Zewail, Proc. Natl. Acad. Sci. USA **107**, 9933 (2010).

[15] Photon-Induced Near-Field Electron Microscopy. B. Barwick, D. J. Flannigan, and A. H. Zewail, Nature **462**, 902 (2009).

[16] 4D Imaging of Transient Structures and Morphologies in Ultrafast Electron Microscopy. B. Barwick, H. S. Park, O.-H. Kwon, J. S. Baskin, and A. H. Zewail, Science **322**, 1227 (2008).

[17] Imaging of transient structures using nanosecond in situ TEM. Kim J S, Lagrange T, Reed B W, Taheri M L, Armstrong M R, King W E, Browning N D, Campbell G H, Science **321**, 1472-1475 (2008).

[18] P. Musumeci, J. T. Moody, C. M. Scoby, M. S. Gutierrez, M. Westfall. Laser-induced melting of a single crystal gold sample by time-resolved ultrafast relativistic electron diffraction. APL **97** (2010).

[19] Four-dimensional ultrafast electron microscopy. Lobastov, V. A., R. Srinivasan, Zewail, A. H., PNAS **102** 7069, (2005).

[20] Atomic-Scale Imaging in Real and Energy Space Developed in Ultrafast Electron Microscopy. H. S. Park, J. S. Baskin, O.-H. Kwon, and A. H. Zewail, Nano Lett. **7**, 2545 (2007).

[21] Single-shot dynamic transmission electron microscopy. T. LaGrange, et al. Appl. Phys. Lett. **89** 044105 (2006).

[22] Nanosecond time-resolved investigations using the in situ of dynamic transmission electron microscope (DTEM). Thomas LaGrange, Geoffrey H. Campbell, B.W. Reed, Mitra Taheri, J. Bradley Pesavento,Judy S. Kim, Nigel D. Browning Ultramicroscopy **108**, 1441 (2008).

[23] B. Reed et al., Rev. Sci. Inst. 81, 053706 (2010).

[24] Implications for Ultrafast Reflection Electron Diffraction from Temporal and Spatial Evolution of Transient Electric Fields. Hyuk Park and J.M. Zuo, MRS Proceedings **1230**, (2011).

[25] Structural dynamics and transient electric-field effects in ultrafast electron diffraction from surfaces. S. Schaefer, W. Liang, A.H. Zewail. Chem. Phys. Lett. **493** 11 (2010).

[26] Photon-induced near-field electron microscopy (PINEM): theoretical and experimental. Sang Tae Park, Milo Lin and Ahmed H Zewail, New J. Phys. **12** 123028, (2010).

[27] Relativistic Effects in Photon-Induced Near Field Electron Microscopy. S.T. Park, A.H. Zewail, J. Phys. Chem. A **116** 11128 (2012).

[28] Subparticle ultrafast spectrum imaging in 4D electron microscopy. A. Yurtsever, R. M. van

der Veen, A. H. Zewail, Science, **335**, 59-64 (2012).

[29] Entangled Nanoparticles: Discovery by Visualization in 4D Electron Microscopy A. Yurtsever, J.S. Baskin, A.H. Zewail, Nano Lett. **12** 5027 (2012).

[30] Direct Visualization of Near-Fields in Nanoplasmonics and Nanophotonics A. Yurtsever, A.H. Zewail, Nano Lett. **12** 3334 (2012).

[31] Chirped imaging pulses in four-dimensional electron microscopy: femtosecond pulsed hole burning. S.T. Park, O.H. Kwon, A.H. Zewail, New J. Phys **14** 053046 (2012).

[32] Enhancing image contrast and slicing electron pulses in 4D near field electron microscopy. S.T. Park, A.H. Zewail Chem. Phys. Lett. **521** 1 (2012).

[33] Electronic structure of MnSi: The role of electron-electron interactions. F. Carbone et al. Phys. Rev. B. **73** 085114 (2006)
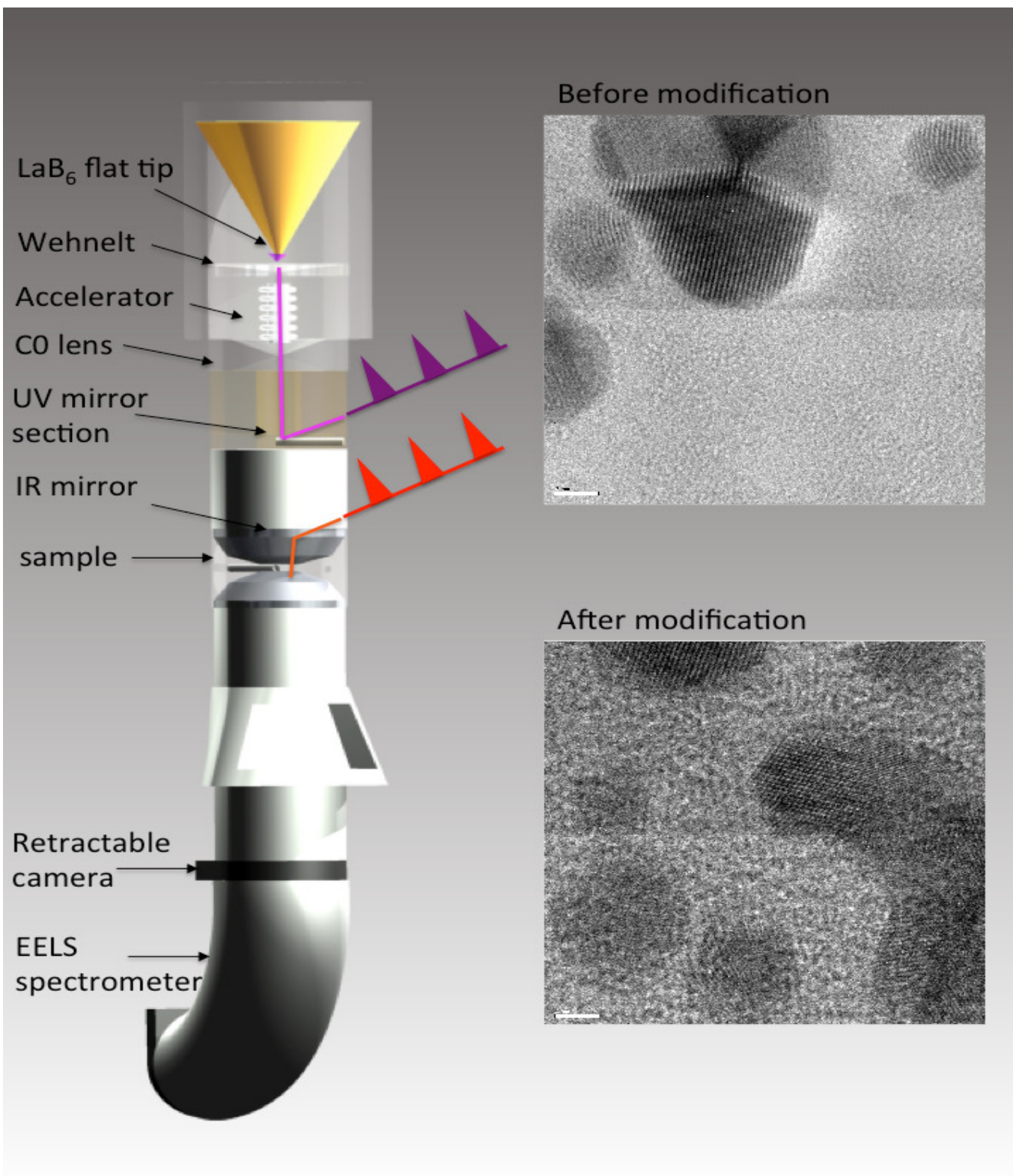
FIG. 1. Modified TEM: the critical sections where conventional parts have been modified are transparent. In the right panel a static atomic resolution image taken on a gold nano-particle TEM resolution standard is shown before and after the modification of the instrument.
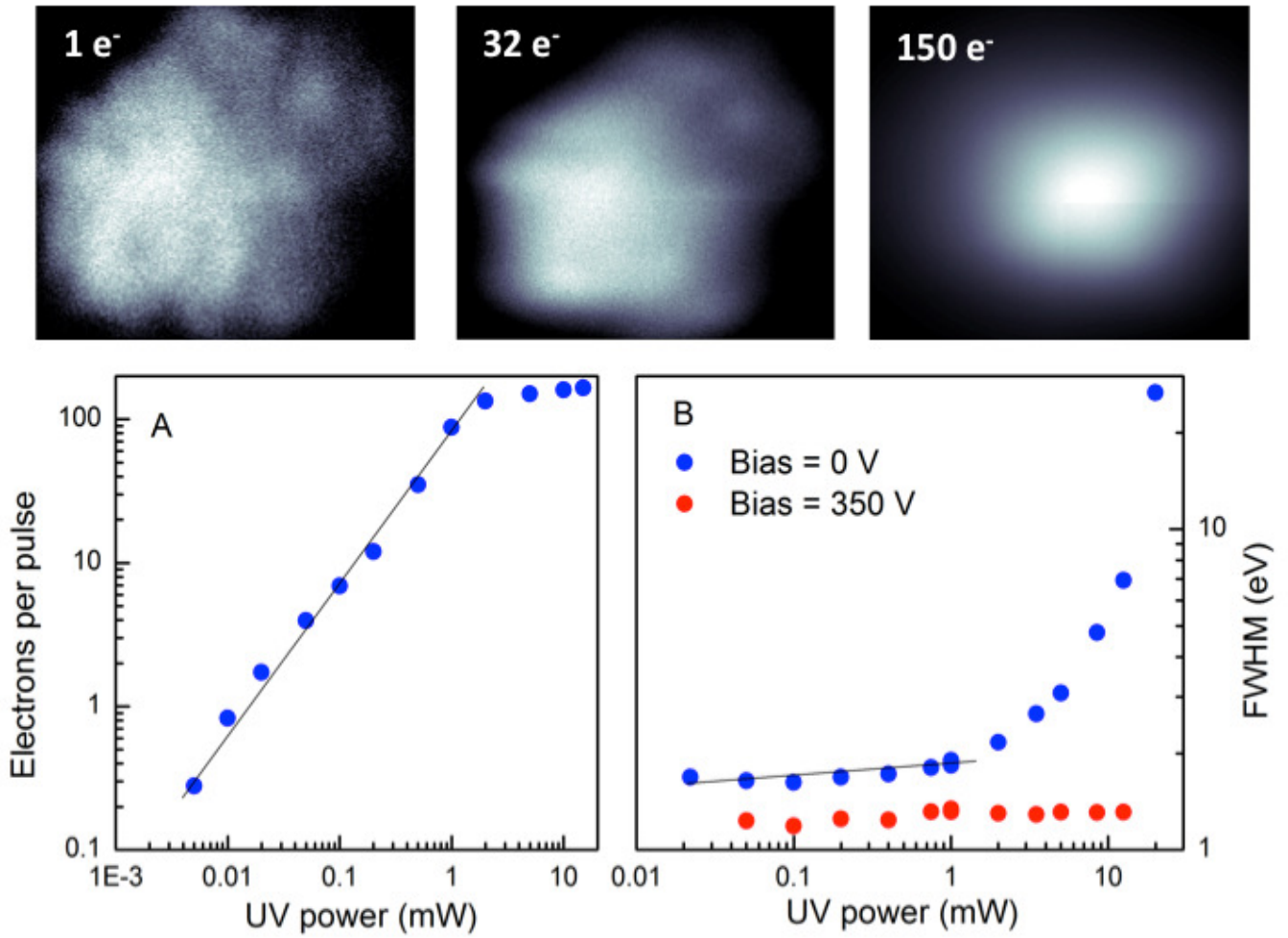
FIG. 2. A. Beam current as a function of UV power. B. Dependence of the FWHM of the ZL peak on the UV power for two different Wehnelt bias voltages. In the top panels of the figure, the images of the tip taken for three different illuminating UV powers are shown.
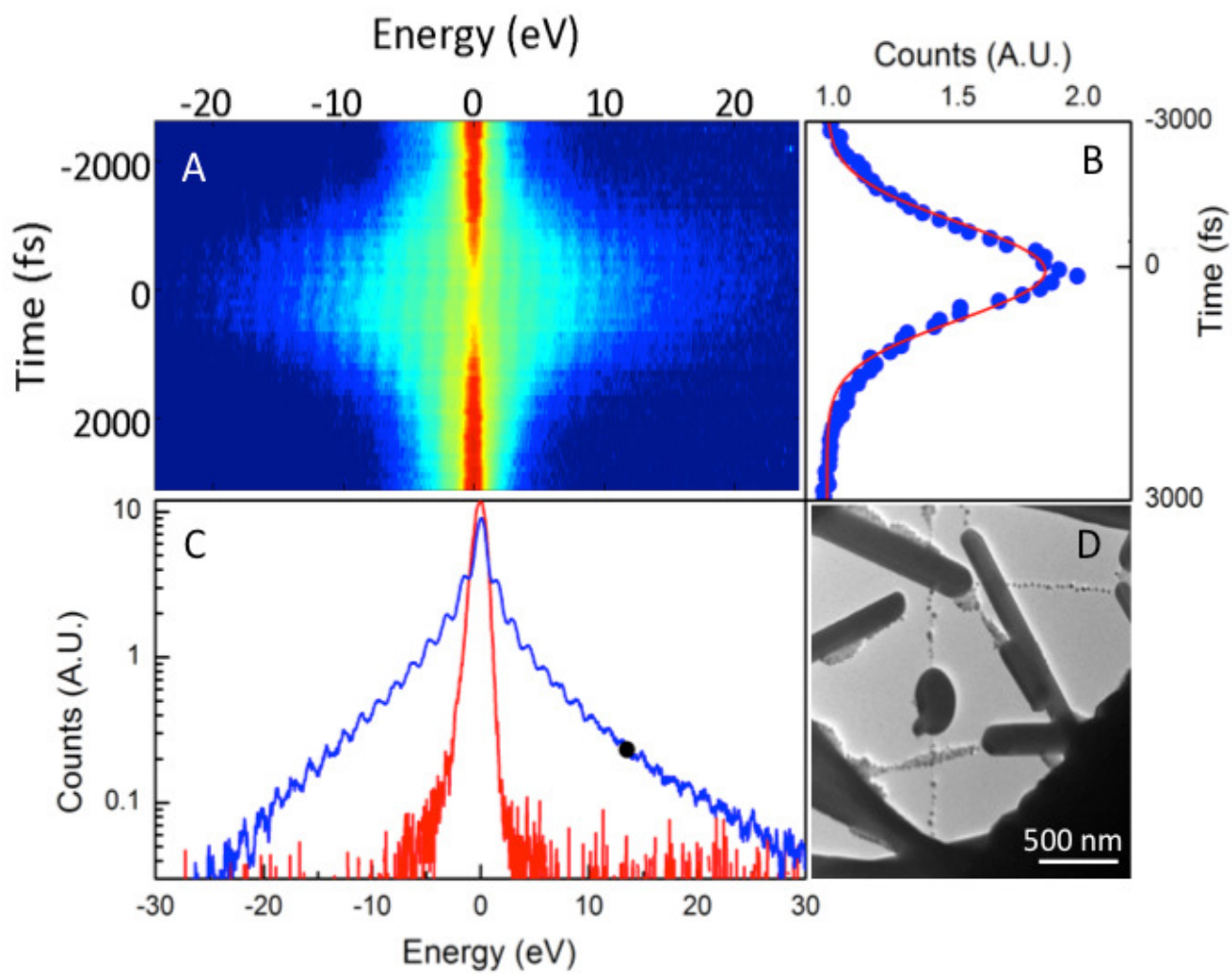
FIG. 3. A Time/energy landscape of the PINEM effect on silver nanotubes. B temporal profile of one of the PINEM sidebands. C Energy profile of the PINEM spectrum. D Image of the silver nanowires.
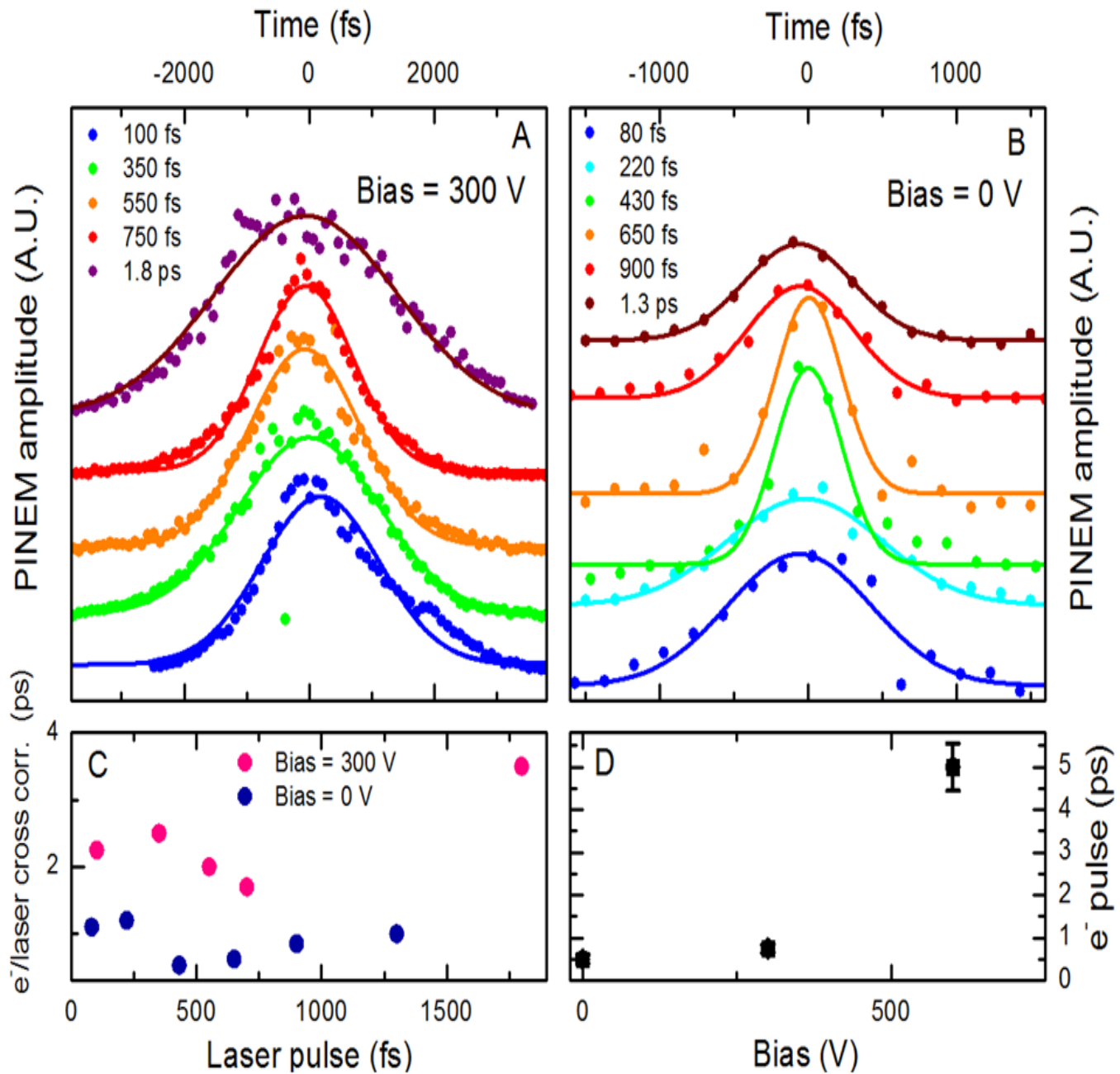
FIG. 4. A Temporal profile of the amplitude of a PINEM sideband as a function of the laser pulses duration at a bias voltage of 300 V. The peak intensity of the pump is kept constant. B Temporal profile of a PINEM sideband as a function of the laser pulses duration at a bias voltage of 0 V. C FWHM of the PINEM temporal profile as a function of the laser pulse duration for two bias voltages. C The shortest electron pulse duration obtained at the different bias voltages is plotted against the bias.